Solid State Ionics 406 (2024) 116482

Contents lists available at ScienceDirect

Solid State Ionics

journal homepage: www.elsevier.com/locate/ssi

Using *in operando* impedance spectroscopy technique to unravel the sintering process evolution of Bi_2O_3:LATP cold-sintered solid electrolyte

Andrés Mormeneo-Segarra [a,b], Sergio Ferrer-Nicomedes [a,b], Sonia Simon [a,b], Nuria Vicente-Agut [a,b,*], Juan Carlos Jarque-Fonfría [a,b], Antonio Barba-Juan [a,b]

[a] Department of Chemical Engineering, Universitat Jaume I, 12071 Castelló, Spain
[b] Institute of Ceramic Technology, Universitat Jaume I, 12071 Castelló, Spain

ARTICLE INFO

Keywords:
Cold sintering process
Solid-ceramic electrolyte
Ionic conductivity
In operando impedance

ABSTRACT

A NASICON-type $Li_{1+x}Al_xTi_{2-x}(PO_4)_3$ (LATP) cold-sintered solid electrolyte is reported with a dense structure, as a possible alternative the commonly recognized liquid organic electrolytes. A low-temperature sintering technology (below 200 °C) with a sintering additive, aid of acid solvent and high pressure is originally developed for preparing the solid electrolyte. In addition, the setup has been designed using *in operando* impedance technique simultaneously, the Cold Sintering Process (CSP) is monitored in order to explore the mechanism are taking place during the densification. As a result, an ionic conductivity as high as $4.48{\cdot}10^{-5}$ S·cm^{-1}, with a relative density of ~82% has been achieved for 2 wt% Bi_2O_3 and 25 wt% 3 M acid acetic solution, LATP powder, and sintered under 700 MPa and at 150 °C, reaching the highest value in published peer-reviewed literature. The cold-sintered ceramics without post-annealing high temperature treatments present kinetics limitations due to intergranular regions. Therefore, this bottleneck must be studied and overcome to achieve higher ionic conductivities at low temperatures.

1. Introduction

Lithium titanium aluminium phosphate ($Li_{1+x}Al_xTi_{2-x}(PO_4)_3$, LATP) is a NASICON (Sodium Super Ionic Conductor)-type and has emerged as a promising solid-state electrolyte (SSE) due to its high ionic conductivity, excellent chemical stability against O_2/H_2O in air, high mechanical strength, a superior chemical compatibility with high-voltage cathode materials, and low cost of the raw materials [1]. In terms of Li^+ ion conductivity, $Li_{1.3}Al_{0.3}Ti_{1.7}(PO_4)_3$ (x = 0.3) has the highest conductivity among different LATP derivatives because the structural modifications of the $LiTi_2(PO_4)_3$ crystal by heteroatom doping with Al^{3+} increases the strength of the Ti—O bond, and reduces the Li—O bond in the microstructure. This phenomenon leads to an improved ionic conductivity up to $1.0{\cdot}10^{-3}$ S cm^{-1}, for crystalline and dense LATP (x = 0.3) at room temperature [2]. To improve the ionic conductivity of this family of materials, many strategies have been studied, including the elemental replacement of the Ti^{4+} by other cations in order to avoid the titanium reduction in contact with lithium metal [3], different mythologies, such as the combination of tape casting with a CSP [4] or the addition of sintering aids (e. g. TeO_2 [5], Li_3PO_4 glass [6], $Li_2CO_3{\cdot}Bi_2O_3$ [7] and $LiBF_4$ [8]). All of them are approaches that have been proposed to be carried out in traditional sintering (temperatures around 1000 °C). Therefore, the strategy to improve the conductivity is to promote sintering densification. Leng et al. showed that the Bi_2O_3 sintering additive (with a low melting point of 820 °C) can be used to enhance the density and conductivity of a Mg-doped NASICON ($Na_{3.256}Mg_{0.128}Zr_{1.872}Si_2PO_{12}$) combining CSP and Bi_2O_3 aid for the first time [9]. In that study, Bi_2O_3 sintering additive was selected to investigate its effects on the crystal structure, microstructure, and ionic conductivity of LATP ceramic electrolytes, by means of a disruptive sintering technology: Cold Sintering Process, which had been recently developed by Randall and co-workers [10–12]. This technique allows to densify a wide variety of materials under high uniaxial pressure and at low temperature (below 300 °C) in short time. The densification process is based on a dissolution-precipitation process through a Transient Liquid Phase (TLP), which dissolves the grain boundaries, facilitating the mass transport and thus sintering by precipitation.

All in all, the effect of introducing a sintering aid to densify LATP by CSP has not been systematically examined yet. Thus, this study aimed to investigate the effect of Bi_2O_3 additive on the structure and ionic

* Corresponding author at: Department of Chemical Engineering, Universitat Jaume I, 12071 Castelló, Spain.
E-mail address: vicenten@uji.es (N. Vicente-Agut).

https://doi.org/10.1016/j.ssi.2024.116482
Received 10 October 2023; Received in revised form 25 January 2024; Accepted 30 January 2024
Available online 2 February 2024

conductivity of LATP cold-sintered solid electrolytes monitoring its electrical behaviour by *in operando* impedance test.

2. Experimental

The LATP powder was synthesized by solid-state reaction. Al_2O_3 (Alfa Aesar, 99%), TiO_2 (Sigma-Aldrich, 99.8%), $NH_4(H_2PO_4)$ (Sigma-Aldrich, 99.99%) and Li_2CO_3 (Sigma-Aldrich, 99.99%) were purchased and used without further purification. In a typical batch synthesis, stoichiometric amounts of the raw materials were weighed and mixed via ball milling with zirconia balls and absolute ethanol as solvent in mass proportion 1:14:5 for six hours in a Pulverisette 5 (Fritsch). The mixture was dried in a vacuum oven at 80 °C for 12 h, after that, the calcination (at 340 °C, for two hours), and followed by the solid-state reaction at 900 °C for four hours. The obtained LATP powder was milled to obtain a particle size of ~0.20 μm, and dried under the same previous conditions. A more detailed experimental procedure can be found in the authors' previous publication [13].

Bismuth oxide (Alfa Aesar, 99.999%) was dissolved in an acetic acid solution 3 M (HAc, Alfa Aesar, 99,7%) that was used as a flux to dissolve the grain boundaries acting as the TLP for the CSP. The synthesized LATP was ground by hand with a mortar and pestle and then mixed with the TLP. Pellets were prepared with different weight percentages of Bi_2O_3 and constant percentage of acetic acid solution. In a previous study, it was proven that the optimum TLP content of acetic acid 3 M was 25 wt% [12]. The prepared powder was then transferred into a 10 mm die between the blocking layers, and three following deaerations were applied by uniaxially pressing (150, 330, and 500 MPa at room temperature). Finally, the cold-sintered specimens were prepared at a pressure of 700 MPa, and the temperature was gradually increased from room temperature to 150 °C, and after a 90 min dwell, a natural cooling process took place. The *in operando* impedance measurement, which is based on the system proposed by Hérisson de Beauvoir [14], was carried out along the CSP of the LATP solid-state electrolytes, and allowed to study the behaviour of the samples during the process evolution. At the end of the sintering process, the pressure is removed, and an impedance spectrum is recorded to study the effect of pressure on the electrical properties in the same setup as the CSP. The setup is shown in Fig. 1 with its correspondent pressure and temperature program. Impedance measurements were performed potentiostatically at different temperatures within the frequency range from 1 MHz to 10 Hz. A Multi Autolab M204 potentiostat from AUTOLAB equipped with an impedance module was employed.

The structures of the prepared powders and the samples obtained were characterized by XRD (Advance diffractometer, Bruker Theta-Theta, Germany), between 5 and 90 degrees, and SEM (FEG-SEM Quanta 200F) to study the changes that have occurred at microstructural level combined with the specimens' relative density (ϕ) defined as the quotient of the real and the theorical density. Sample's density was evaluated by Arquimedes method in mercury. The theoretical density value of 2.91 g cm^{-3} was determined by helium pycnometry.

3. Results and discussion

3.1. *In operando* electrochemical impedance spectroscopy of *x*-Bi_2O_3: $Li_{1.3}Al_{0.3}Ti_{1.7}(PO_4)_3$

Fig. 2.a shows the Nyquist spectra plots obtained at the end of the sintering process for the different prepared compositions without and with 1, 2, 3, 4 and 5 wt% Bi_2O_3, and the equivalent circuit used to modelize them. Note how the frequency response of the electrolytes reveal two main features at different time constants associated with the corresponding specific electrochemical mechanisms: a semicircle obtained at high-frequencies (related to the grain resistance and grain boundary resistance), and a tilted line at low frequencies (that correlates to the blocking layer). The relevant points are marked out in Fig. 2.a. The equivalent circuit consisting of $(R_g)(R_{gb}CPE_1)(R_1\ CPE_2)C_1$. R_g, R_{gb}, CPE_1, and $(R_1\ CPE_2)C_1$ represent grain resistance, constant phase element, grain-boundary resistance, and elements which fit impedance related to Li^+ diffusion within the electrolyte, respectively.

Some of the several registered impedance spectra during the maximum temperature plateau and the cooling process, are shown in the Fig. 2.b for the 2 wt% Bi_2O_3:LATP electrolyte. In the expanded view of the spectra recorded during the plateau at maximum temperature (Fig. 2.c) it can be seen that the total resistance, including both the bulk and the grain boundary resistance, increases with time once the steady state at the maximum temperature is reached. Thus, densification is taking place since the TLP has dissolved part of the grain boundary, and due to its evaporation, the LATP and the sintering aid precipitate allowing the densification. At the same time, it is also observed that the blocking layer becomes more resistive. When the temperature decreases to room temperature, as might be expected, the resistance increases.

By fitting the equivalent circuit to the impedance data for different aid content, the R_{tot} values are obtained and can be seen in Table S1. This yielded the R_g values within the range of 5–115 Ω corresponding to an ionic conductivity from $3.46{\cdot}10^{-2}$ - $1.58{\cdot}10^{-3}$ S cm^{-1} approaching the one of the single-crystal LATP materials [15]. This allowed to calculate the total ionic conductivity by the Eq. (1), as it was demonstrated in the previous publications of the research group [13,16]:

$$\sigma_{tot} = \frac{L}{S{\cdot}(R_{tot})} \tag{1}$$

where σ_{tot} is the total ionic conductivity, L is the thickness of the sample (1.35 ± 0.05 mm) and S the surface area (76.51 mm^2, constant). Each ionic conductivity, from the last measurement at 150 to 30 °C, was calculated and plotted vs. temperature in Fig. 3.a, where every curve corresponds to a Bi_2O_3 content, and each point of a curve corresponds to a spectrum registered *in operando* at a CSP time during the cooling stage.

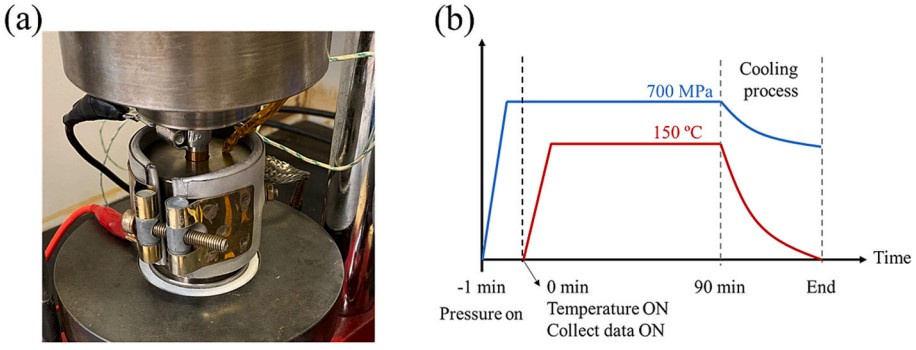

Fig. 1. (a) Setup employed to monitor the Cold Sintering Process evolution by in operando Electrical Impedance Spectroscopy measurements; (b) Evolution of the pressure and temperature program during the CSP.

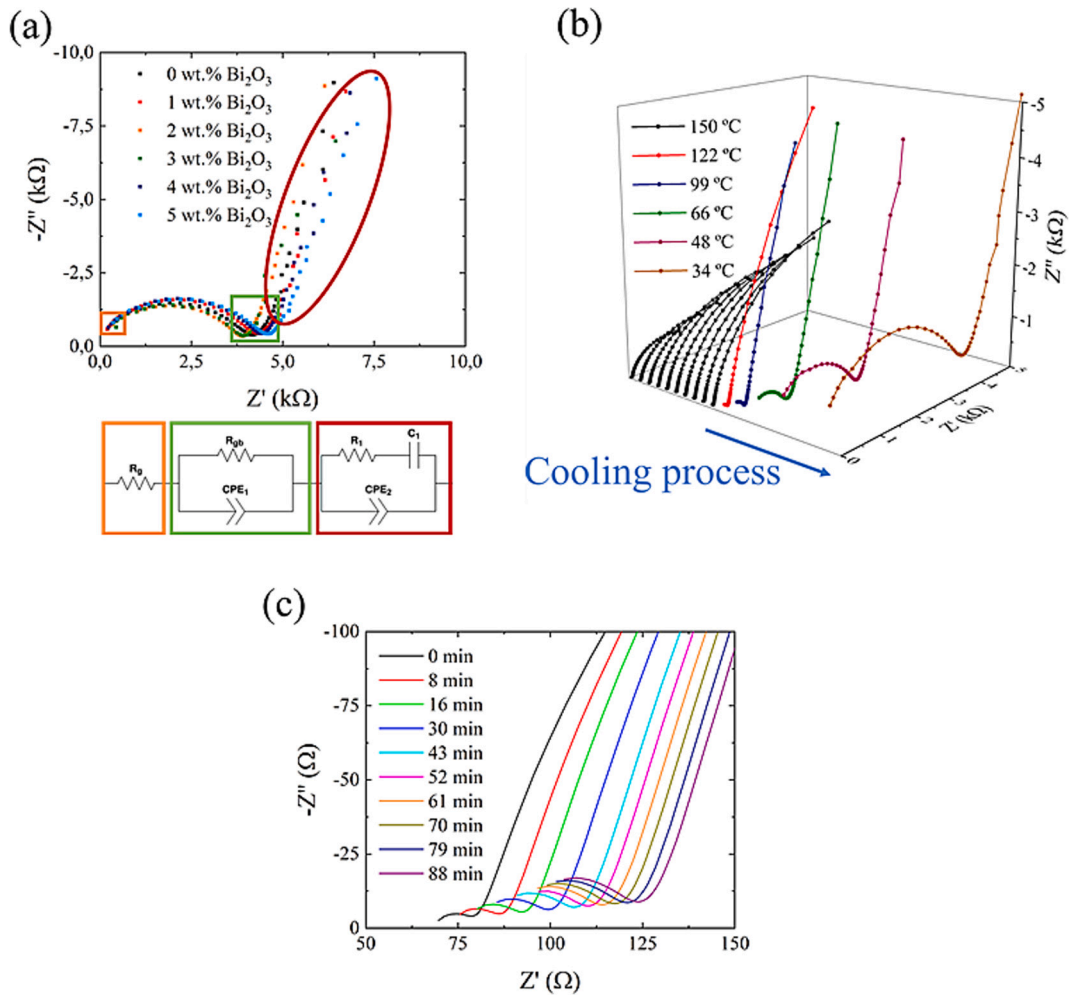

Fig. 2. (a) Nyquist plots (measured at room temperature) of the cold-sintered x-Bi_2O_3-LATP samples, where main points have been marked out: R_g, R_{gb} and blocking layer to link with the equivalent circuit for fitting, which is displayed under the plot. (b) Impedance spectra recorded during the cooling of the electrolyte whose composition is 2 wt% Bi_2O_3-LATP after the CSP. (c) Expanded view of impedance spectra recorded during maximum temperature dwell.

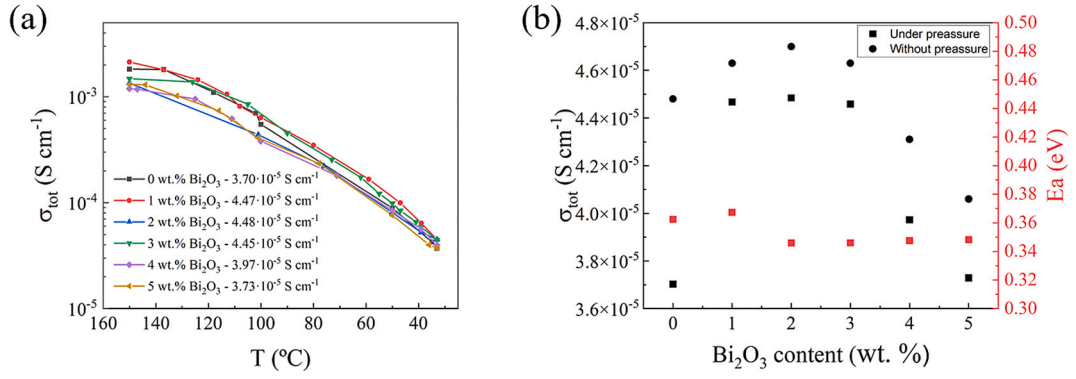

Fig. 3. (a) Calculated total conductivities of x-Bi_2O_3-LATP sintered at different temperatures during the cooling process. (b) Total ionic conductivities (under P and without P) and activation energies for the different Bi_2O_3 contents studied.

Herein, it can be observed that the highest conductivity at room temperature is reached by a composition with 2 wt% bismuth oxide, $4.48{\cdot}10^{-5}$ S cm^{-1}, although it should be noted that the values of 1 and 3 wt%, with $4.47{\cdot}10^{-5}$ and $4.45{\cdot}10^{-5}$ S cm^{-1}, respectively, are very close. Then, considering the experimental error (~5%), the optimal additive content could not be discerned, although it is possible to narrow down the range where it is found. All of them are in the same order of magnitude as reported in bibliography for cold-sintered LATP with different additives, and without post-annealing (water, NMP, and HAc) [17,18].

Cold-sintered pieces with the same density do not have the same conductivity, so achieving a high density is not enough to guarantee high conductivity. The improvement of the ionic conductivity mainly comes from the grain boundary characteristics, shown in Fig. 3.a-b.

Understanding the factors limiting the ionic conductivity of cold-sintered samples is necessary for optimizing the solid electrolytes to make them suitable for solid-state batteries.

On the basis of σ_{tot} from 150 to 30 °C (cooling process) the activation energies ($E_{a,tot}$) of the sintered electrolytes pellets are calculated. These energies are related to the lithium-ion migration rate along the unoccupied sites, and can be obtained by means following the modified Arrhenius law (Eq. (2)), which establishes the relationship among conductivity and temperature [19]:

$$\sigma_{tot} \cdot T = A_{tot} \cdot e^{-\frac{E_{a,tot}}{k_B \cdot T}} \quad (2)$$

where A_{tot} is the pre-exponential factor, which contains the entropy of migration and the charge carriers, $E_{a,tot}$ the total activation energy, k_B the Boltzmann constant and T the absolute temperature. High conductivities are reached when total activation energy is low, and the concentration of mobile ion carries is high.

The fitted data obtained from the impedance spectra (Table S1) yields the $E_{a,tot}$ values by applying Eq. (2), which are shown in Fig. 3.b. It can be seen that the total activation energy for LATP is 0.36 eV, which is an agreement with the value reported previously [20]. Despite 1, 2 and 3 wt% Bi_2O_3 have comparable ionic conductivity, their total activation energies point out that are energetically favourable for Li^+ conduction:

2 wt% Bi_2O_3 (0.35 eV) or higher in the studied range.

Therefore, if both the conductivity and the activation energy are

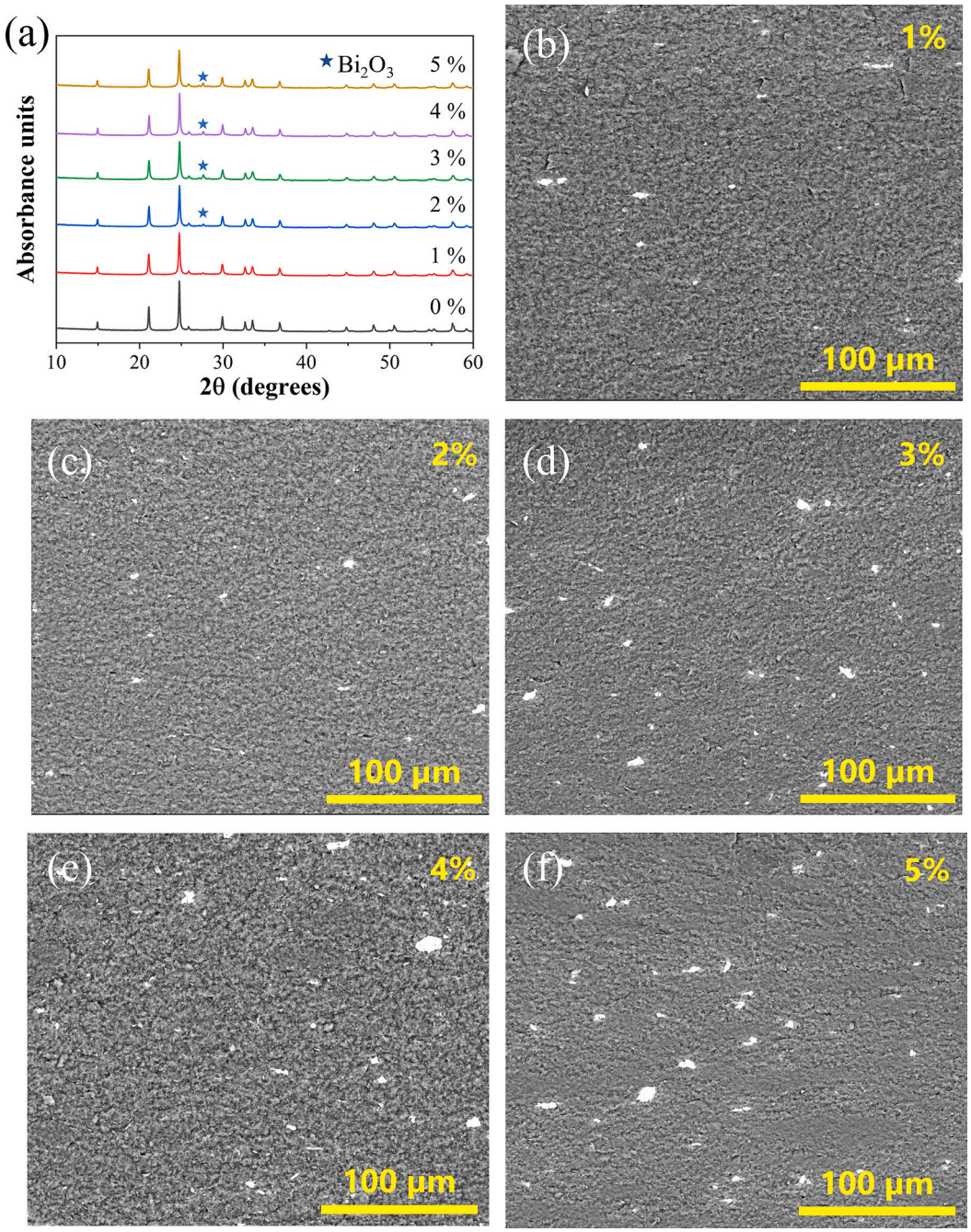

Fig. 4. (a) XRD patterns of the cold-sintered x-Bi_2O_3:LATP samples with 1, 2, 3, 4, and 5 wt% Bi_2O_3 sintering additive, along with the powder pattern; (b-f) SEM micrographs of the fractured surfaces of the x-Bi_2O_3:LATP samples: (b) 1 wt%, (c) 2 wt%, (d) 3 wt%, (e) 4 wt%, and (f) 5 wt% Bi_2O_3 sintering aid, respectively, under 700 MPa at 150 °C for 90 min.

regarded, it can be reported that the bismuth oxide content that favours sintering, increases the conductivity and decreases the activation energy, is 2 wt% content. When the pressure is removed, it is observed that the conductivity increases slightly, following the same trend as under sintering pressure. This is consistent with reports in the literature. [21]

3.2. Structure analysis of Bi_2O_3:$Li_{1.3}Al_{0.3}Ti_{1.7}(PO_4)_3$

High relative densities of ~82% were achieved for cold-sintered x-Bi_2O_3:LATP pellets with different sintering aid content, all processed under 700 MPa at 150 °C for 90 min, in comparison with only ~72% densities for the green pressed samples at an identical pressure at room temperature. Fig. 4.a shows XRD patterns of the sintered LATP electrolytes with different sintering aid content (0, 1, 2, 3, 4 and 5 wt%). All pellets exhibit a primary phase $Li_{1.3}Al_{0.3}Ti_{1.7}(PO_4)_3$ (ICSD 14585). No secondary phases of the LATP are present after addition, and it can clearly be observed that there is no peak coming from the Bi_2O_3 below 2 wt% specimens.

The microstructures of the cold-sintered electrolytes are shown in Fig. 4. b-f. These are typical sintering microstructures including particle packing, indicating that the densification has taken place during CSP. It should be noted that there is no grain growth when this sintering technique is used, or at least it is imperceptible (nanometric level) [10]. The development of the microstructure is in line with the increasing addition of Bi_2O_3: the higher the additive content, the higher the number of agglomerates and white particles, where these bright zones are relative to the bismuth species and the darker ones the LATP.

Probably, these agglomerates were formed by deformation and inhomogeneity, since the acetic acid solution is not able to dissolve all Bi_2O_3 particles and distribute around the particles of the starting powder. The best homogenization of the mixture is reached with 2 wt% Bi_2O_3, ensuring well cold-sintered bodies with proper final properties. As the content increases, areas of agglomerates appear, more notable for 5-Bi_2O_3-LATP, indicating that the TLP has not been distributed among all the LATP grains, and thus the dissolution-precipitation process, on which the CSP is based, has not occurred. This phenomenon results in a decrease in ionic conductivity as it has been seen and has no impact on densification.

4. Conclusions

The fast Li^+ conductor LATP has been successfully sintered by Cold Sintering Process by adding a TLP, which based on Bi_2O_3 dissolved in a 3 M acetic acid solution (25 wt%), achieving ~82% of the relative density under 700 MPa and at 150 °C for 90 min, without any post-annealing treatment.

For this purpose, different percentages of Bi_2O_3 were added to the LATP powders, from 0 to 5 wt%, and compared based on their electrical characteristics and the morphology of their microstructures. According to the impedance measurements of the samples it was possible to observe that the activation energy presents a minimum for the 2 wt% Bi_2O_3 sample. Although, this sample does not present a significant enhancement of the densification, it was found to have increased the ionic conductivity of the cold-sintered LATP samples from $\sim 3.70 \cdot 10^{-5}$ to $\sim 4.48 \cdot 10^{-5}$ S cm^{-1} under pressure and from $\sim 4{,}48 \cdot 10^{-5}$ to $\sim 4.70 \cdot 10^{-5}$ S cm^{-1} without pressure, while simultaneously decreased the total activation energy from ~0.36 to 0.35 eV, for 0 and 2 wt% Bi_2O_3, respectively. It should be noted that this sintering aid increases the ionic conductivity via modifying the grain boundary region. Compared to the microstructure of different compositions, a higher wt% of Bi_2O_3, resulted in a higher number of aggregates to larger agglomerates across the sample, being the most homogeneous sample the 2-Bi_2O_3-LATP. This have been possible to the combination of the three cornerstones: the Bi_2O_3 additive, CSP and in operando impedance spectroscopy to monitor the sintering process evolution, this lead to a better understanding of the Cold Sintering Process, and provide a first impression on how the properties are evolving by impedance spectroscopy.

This paper demonstrates that the electrical properties of a solid electrolyte are determined by the interface formed after sintering and is the result of a balance between densification, microstructure and, in this case, the Bi_2O_3 additive, which has a positive effect on ionic conductivity, but more significantly on activation energy of the electrolyte. In other words, a key point for further research is to find a way to influence both properties at the same time, and to improve the resistance of the interfacial zone as it has the greatest contribution.

CRediT authorship contribution statement

Andrés Mormeneo-Segarra: Writing – review & editing, Methodology, Investigation, Formal analysis, Data curation. **Sergio Ferrer-Nicomedes:** Investigation, Formal analysis, Data curation. **Sonia Simon:** Methodology, Data curation. **Nuria Vicente-Agut:** Writing – review & editing, Writing – original draft, Supervision, Project administration, Methodology, Investigation, Conceptualization. **Juan Carlos Jarque-Fonfría:** Writing – review & editing, Supervision, Investigation, Formal analysis. **Antonio Barba-Juan:** Writing – review & editing, Validation, Supervision.

Declaration of competing interest

The authors declare the following financial interests/personal relationships which may be considered as potential competing interests:

Nuria Vicente-Agut reports financial support was provided by University Jaume I. Andres Mormeneo-Segarra reports financial support was provided by Valencia Department of Education Culture and Sport. Sergio Ferrer-Nicomedes reports financial support was provided by Valencia Department of Education Culture and Sport. Antonio Barba-Juan reports financial support was provided by Valencia Department of Education Culture and Sport. Antonio Barba-Juan reports financial support was provided by Spain Ministry of Science and Innovation.

Data availability

Data will be made available on request.

Acknowledgements

All authors are grateful to the Generalitat Valenciana for funding their research projects within the framework of Pla Complementari “Programa de Materials Avançats”, 2022 (MFA/2022/030). A.B.-J. acknowledges the financial support from Ministerio de Ciencia e Innovación (Spain) under project no. MCIN/AEI/10.13039/501100011033. A.M.-S. and S.F.-N. thank Generalitat Valenciana through FPI Fellowship Program (ACIF/2020/294 and ACIF/2021/050). N.V.-A. acknowledges funding by Universitat Jaume I under the grant number POSDOC/2020/04. The authors also acknowledge SCIC and IUTC from UJI.

Appendix A. Supplementary data

Supplementary Material with complementary information about experimental procedure and results is available in the online version of this article. Supplementary data to this article can be found online at [https://doi.org/10.1016/j.ssi.2024.116482].

References

[1] W. Xiao, J. Wang, L. Fan, J. Zhang, X. Li, Recent advances in Li1+xAlxTi2−x(PO4)3 solid-state electrolyte for safe lithium batteries, Energy Storage Mater. 19 (2019) 379–400, https://doi.org/10.1016/j.ensm.2018.10.012.

[2] H. Aono, E. Sugimoto, Y. Sadaoka, N. Imanaka, G. Adachi, Ionic conductivity of solid electrolytes based on lithium titanium phosphate, J. Electrochem. Soc. 137 (4) (1990) 1023, https://doi.org/10.1149/1.2086597.
[3] R. DeWees, H. Wang, Synthesis and properties of NaSICON-type LATP and LAGP solid electrolytes, ChemSusChem 12 (16) (Aug. 2019) 3713–3725, https://doi.org/10.1002/cssc.201900725.
[4] N. Hamao, Y. Yamaguchi, K. Hamamoto, Densification of a NASICON-type LATP electrolyte sheet by a cold-sintering process, Materials 14 (16) (2021), https://doi.org/10.3390/ma14164737.
[5] X. Zhao, Y. Luo, X. Zhao, Effect of TeO2 sintering aid on the microstructure and electrical properties of Li1.3Al0.3Ti1.7(PO4)3 solid electrolyte, J. Alloys Compd. 927 (2022) 167019, https://doi.org/10.1016/j.jallcom.2022.167019.
[6] Y. Zhong, J. Luo, F. Shang, G. Chen, Preparation, microstructure and ionic conductivity of Li1.3Al0.3Ti1.7(PO4)3/50Li2O–50P2O5 glass ceramic electrolytes, J. Mater. Sci. Mater. Electron. 33 (10) (2022) 7869–7882, https://doi.org/10.1007/s10854-022-07937-z.
[7] Y. Luo, H. Gao, X. Zhao, Insights into the sinterability and electrical properties of Li1.3Al0.3Ti1.7(PO4)3-(Li2CO3·Bi2O3) composite electrolytes, Ceram. Int. 48 (6) (2022) 8387–8394, https://doi.org/10.1016/j.ceramint.2021.12.045.
[8] L. Dai, J. Wang, Z. Shi, L. Yu, J. Shi, Influence of LiBF4 sintering aid on the microstructure and conductivity of LATP solid electrolyte, Ceram. Int. 47 (8) (2021) 11662–11667, https://doi.org/10.1016/j.ceramint.2021.01.004.
[9] H. Leng, J. Nie, J. Luo, Combining cold sintering and Bi2O3-activated liquid-phase sintering to fabricate high-conductivity Mg-doped NASICON at reduced temperatures, J. Mater. 5 (2) (2019) 237–246, https://doi.org/10.1016/j.jmat.2019.02.005.
[10] H. Guo, A. Baker, J. Guo, C.A. Randall, Cold sintering process: a novel technique for low-temperature ceramic processing of ferroelectrics, J. Am. Ceram. Soc. 99 (11) (Nov. 2016) 3489–3507, https://doi.org/10.1111/jace.14554.
[11] A. Ndayishimiye, S.H. Bang, Christopher, J. Spiers, C.A. Randall, Reassessing cold sintering in the framework of pressure solution theory, J. Eur. Ceram. Soc. 43 (1) (2023) 1–13, https://doi.org/10.1016/j.jeurceramsoc.2022.09.053.
[12] S.S. Berbano, J. Guo, H. Guo, M.T. Lanagan, C.A. Randall, Cold sintering process of Li1.5Al0.5Ge1.5(PO4)3 solid electrolyte, J. Am. Ceram. Soc. 100 (5) (May 2017) 2123–2135, https://doi.org/10.1111/jace.14727.
[13] A. Mormeneo-Segarra, S. Ferrer-Nicomedes, N. Vicente-Agut, A. Barba-Juan, In operando characterization of the ionic conductivity dependence on liquid transient phase and microstructure of cold-sintered Bi2O3-doped Li1.3Al0.3Ti1.7(PO4)3 solid-state electrolyte, Ceram. Int. (2023), https://doi.org/10.1016/j.ceramint.2023.08.333.
[14] T. Hérisson de Beauvoir, P.-L. Taberna, P. Simon, C. Estournès, Cold sintering process characterization by in operando electrochemical impedance spectroscopy, J. Eur. Ceram. Soc. 42 (13) (2022) 5747–5755, https://doi.org/10.1016/j.jeurceramsoc.2022.05.077.
[15] D. Rettenwander, et al., A microcontact impedance study on NASICON-type Li1+xAlxTi2−x(PO4)3 ($0 \leq x \leq 0.5$) single crystals, J. Mater. Chem. A Mater. 4 (4) (2016) 1506–1513, https://doi.org/10.1039/C5TA08545D.
[16] S. Ferrer-Nicomedes, A. Mormeneo-Segarra, N. Vicente-Agut, A. Barba-Juan, Introducing an ionic conductive matrix to the cold-sintered Li1.3Al0.3Ti1.7(PO4)3-based composite solid electrolyte to enhance the electrical properties, J. Power Sources 581 (2023) 233494, https://doi.org/10.1016/j.jpowsour.2023.233494.
[17] M. Vinnichenko, et al., Li-ion conductive Li1.3Al0.3Ti1.7(PO4)3 (LATP) solid electrolyte prepared by cold sintering process with various sintering additives, Nanomaterials 12 (18) (2022), https://doi.org/10.3390/nano12183178.
[18] Y. Liu, et al., Insight into the microstructure and ionic conductivity of cold sintered NASICON solid electrolyte for solid-state batteries, ACS Appl. Mater. Interfaces 11 (31) (Aug. 2019) 27890–27896, https://doi.org/10.1021/acsami.9b08132.
[19] J. R. M. E. Barsoukov, "Impedance spectroscopy: Theory, experiment, and applications." Accessed: Sep. 25, 2023. [Online]. Available: https://www.wiley.com/en-us/Impedance+Spectroscopy%3A+Theory%2C+Experiment%2C+and+Applications%2C+3rd+Edition-p-9781119074083.
[20] S.-P. Shen, et al., Low-temperature fabrication of NASICON-type LATP with superior ionic conductivity, Ceram. Int. 48 (24) (2022) 36961–36967, https://doi.org/10.1016/j.ceramint.2022.08.264.
[21] A. Méry, S. Rousselot, D. Lepage, D. Aymé-Perrot, M. Dollé, Limiting factors affecting the ionic conductivities of LATP/polymer hybrid electrolytes, Batteries 9 (2) (2023), https://doi.org/10.3390/batteries9020087.